IEEE Access
Multidisciplinary | Rapid Review | Open Access Journal

Received 29 May 2024, accepted 29 June 2024, date of publication 9 July 2024, date of current version 29 July 2024.

Digital Object Identifier 10.1109/ACCESS.2024.3425520

RESEARCH ARTICLE

A Compact 2-Port QMSIW Cavity-Backed MIMO Antenna With Varied Frequencies Using CSRR-Slot Angles for WBAN Application

DIVYA CHATURVEDI[1], (Senior Member, IEEE), PRAKASH JADHAV[2], AYMAN A. ALTHUWAYB[3], (Member, IEEE), AND KHALED ALIQAB[3], (Member, IEEE)

[1]Department of ECE, Indian Institute of Information Technology, Pune, India
[2]Department of Mechanical Engineering, SRM University-AP, Amaravati 522502, India
[3]Department of Electrical Engineering, College of Engineering, Jouf University, Sakaka, Al Jowf 72388, Saudi Arabia

Corresponding author: Ayman A. Althuwayb (aaalthuwayb@ju.edu.sa)

The authors extend their appreciation to the Deputyship for Research & Innovation, Ministry of Education in Saudi Arabia for funding this research work through the project number 223202.

ABSTRACT This paper presents a novel design of a compact, low-profile, Substrate Integrated Waveguide (SIW) based Multiple-Input Multiple-Output (MIMO) antenna operating at the 2.45 GHz Industrial, Scientific, Medical (ISM) band. The antenna consists of two quarter-mode (QM) SIW cavity resonators and one diamond-shaped complementary split ring resonator (CSRR) slot etched on each cavity. The unique feature of this geometry is the ability to tune the operating frequency of the dominant mode to a lower frequency range by rotating the slot in the range of 0°-180°. The excitation of both cavities is achieved using microstrip feedlines. By placing both cavities in an orthogonal configuration, a significant isolation level of around -28 dB between the two ports is achieved. MIMO metrics parameters, including the envelope correlation coefficient (ECC) and diversity gain (DG), mean effective gain (MEG), and channel capacity loss (CCL) have been investigated, validating the MIMO capabilities of the proposed design. Due to its compact dimensions, minimal profile, and alignment with the ISM band, the antenna lends itself seamlessly to integration with healthcare devices, facilitating its deployment within Wireless Body Area Network (WBAN) applications. The robust performance of the antenna in the vicinity of the human body has been verified by investigating the S_{11} against frequency on different body parts such as the arm, head, and chest of the voxel phantom. The proposed design has been experimentally tested, and the measured responses closely agree with the simulations. The antenna exhibits a front-to-back ratio better than 10 dB and peak measured gain values of 5.0 dBi.

INDEX TERMS Compact design, ISM band, MIMO antenna, MIMO diversity parameters, microstrip feedline, planar circuit, substrate integrated waveguide, voxel body model.

I. INTRODUCTION

MIMO (Multiple Input Multiple Output) antenna systems are used in wireless communication to improve signal quality and increase data throughput by using several antennas at both the transmitter and receiver sides [1]. These antennas are inherently used to offer antenna diversity that uses multiple antennas to be deployed at both the transmitter and receiver end. The antennas should have different polarizations, orientations, or spatial locations to minimize signal

The associate editor coordinating the review of this manuscript and approving it for publication was Muhammad Usman Afzal.

fading and to improve diversity gain. Generally, increasing the number of antennas in a MIMO system can increase channel capacity, up to a certain point [2]. The antennas, which can cause interference and reduce the effectiveness of the MIMO system. Designing a MIMO antenna presents the challenging task of achieving miniaturization while ensuring higher isolation levels among the channels [3], [4]. In the last decade, Substrate Integrated Waveguide (SIW) has gained popularity in implementation of MIMO antennas due to its cost-effectiveness, unidirectional pattern, and low insertion loss properties. It offers waveguide-like features in planar laminates with a high-quality factor and enhanced power handling. To create compact circuits, half-mode (HM), quarter-mode (QM), and eight-mode (EM) SIW cavities are vital, offering similar benefits as full-mode (FM) SIW in a more compact form [4], [5], [6], [7]. An overview of adaptive antennas, encompassing various aspects such as fundamental principles and space-time channel models is presented in [8]. In [9], a dual-band 28/38 GHz MIMO antenna with two elements is showcased as a potential solution for the forthcoming 5G network. To enhance decoupling between the antenna elements, they are strategically positioned on the top and bottom layers of the substrate. The work [10] introduces a dual-band textile MIMO antenna designed to operate at 2.4 GHz and 5 GHz. By carefully placing a via within the cavity, the second and third modes are modified and combined. In [11], a 4-element planar inverted F-antenna (PIFA) MIMO antenna is designed, and the isolation is improved by around 5 dB by placing slots in ground plane. A 2-element MIMO antenna presented in [12] achieves an isolation of 18 dB by employing a T-shaped slot. A compact MIMO antenna utilizing substrate-integrated waveguide (SIW) technology is proposed, which achieves enhanced bandwidth and high isolation. The bandwidth is expanded by exciting an electromagnetic SIW cavity using a coaxial probe and placing a parasitic cavity in proximity. Utilizing the 1/8th mode of a conventional folded microstrip integrated waveguide (FMSIW) cavity, the work [13] realizes a compact 2 × 2 MIMO antenna. A dual-band self-diplexing 4-port MIMO antenna is demonstrated in [14], wherein the bandwidth is increased in each frequency band through the coupling of odd and even-half-TE_{110} modes. Finally, the work in [15] shows a 2-element MIMO Antenna using optically transparent wired-metal mesh. The SIW-inspired multi-ports antenna employing the polarization diversity features is investigated in [16], [17], and [18]. The isolation is improved by employing a metamaterial structure in [19] and by adding a coupling element to create a cancellation path in [20]. A self-diplexing antenna is realized at two distinct frequency bands in [21] by using a concept of shielded QMSIW cavity.

This article introduces a compact 2-ports MIMO antenna tailored for Wireless Body Area Network (WBAN) applications, operating at 2.45 GHz (2.4-2.5 GHz, 100 MHz) in ISM band. The antenna's size reduction is achieved by utilizing a Quarter-Mode (QM) SIW cavity, minimizing it up to 1/4th of the FMSIW cavity by retaining the quarter-dominant mode

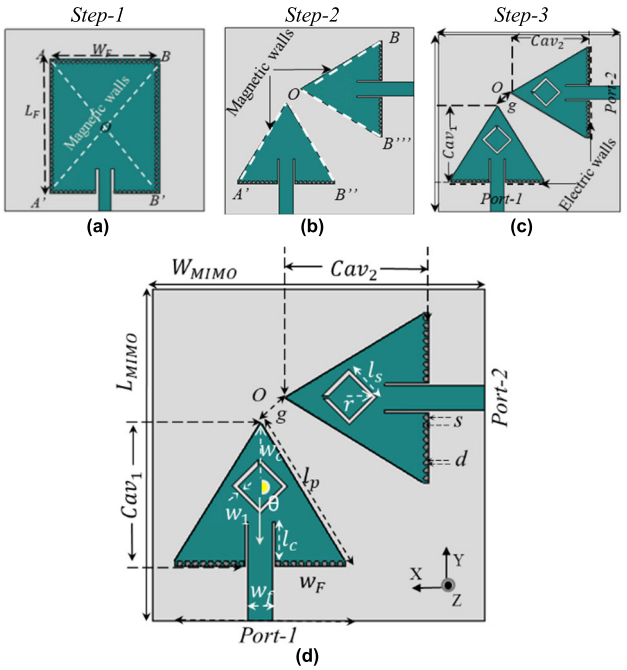

FIGURE 1. Schematic diagram of proposed design (a) FMSIW cavity, (b) QMSIW cavity-backed MIMO antenna without slots (c) Proposed MIMO antenna, (d) Schematic diagram of the proposed antenna, Dimensions ($W_{MIMO} = L_{MIMO} = 54$, $l_p = 33$, $W_F = 31$, $L_F = 49$, $l_s = 7.2$, $w_c = 11.5$, $w_f = 4.4$, w_1 =0.4, $r = 4.8$, $l_c = 7.2$, $s = 1.1$, $d = 0.8$, $g = 5$) (Units: mm).

TE_{110}. Further additional miniaturization is accomplished around 13% by inserting a diamond shaped CSRR slot on the top plane of each QMSIW cavity. The CSRR slot not only aids in miniaturization but also enables tuning the resonant frequency by rotating it. The radiation is launched from the two magnetic open walls of the quarter-TE_{110} mode cavity. To enhance the MIMO performance, the proposed antenna configuration adopts an orthogonal placement of the cavities, resulting in an isolation between ports exceeding around −28 dB.

II. DESIGN, CONFIGURATION, AND ANALYSIS

Fig. 1 depicts the design evolution of the proposed MIMO antenna, which comprises two triangular QMSIW cavities (i.e., *Cav1* and *Cav2*) with diamond shaped CSRR slots etched on each cavity. The steps to design the proposed antenna start from *Step-1, i.e.* a rectangular SIW cavity, as shown in Fig. 1(a). The SIW cavity is accomplished by embedding metallic posts in the dielectric substrate, forming the electric walls. The diameter and pitch of the posts are meticulously selected following the guidelines provided in [16], to prevent energy leakage from the shorting metallic for FMSIW cavity

$$f_{110(\mathrm{FM})} = \frac{c}{2\sqrt{\varepsilon_{reff}}}\sqrt{\left(\frac{1}{W_{F(FM)}}\right)^2 + \left(\frac{1}{L_{F(FM)}}\right)^2} \quad (1)$$

for QMSIW cavity

$$f_{110(\mathrm{QM})} = \frac{c}{2\sqrt{\varepsilon}_{reff}}\sqrt{\left(\frac{1}{2W_{F(QM)}}\right)^2 + \left(\frac{1}{1.6\,L_{F(QM)}}\right)^2} \quad (2)$$

where W_F and L_F are the length and width of the FMSIW cavity.

Initially, the dimensions of the cavity are determined $W_F \times L_F$ mm^2 by using equation (1) to achieve the dominant mode (i.e., TE_{110}) of the FMSIW cavity operating around 3.5 GHz (as shown in *Step-2)*. By taking advantage of the symmetrical E-field distribution of the dominant mode, the cavity is successively divided into four parts along the two diagonals *A-A'* and *B-B'*, respectively (as shown in *Step-1*). The QMSIW cavity preserves the dominant mode and operates at 2.81 GHz. The two open walls act as slots through which radiation gets launched in free space. Thus, two identical quarter-mode SIW cavities are realized maintaining the same mode in the 1/4th part of the full-mode cavity with slight variations in gain and front-to-back ratio. To achieve a 2-elements MIMO antenna each cavity is individually excited with a microstrip feedline, as shown in Fig. 1(b) (as shown in *Step-2)*. The dimensions of the FMSIW and QMSIW cavities for the dominant mode are determined using equations (1) and (2) [14].

The operating frequency for the QMSIW cavity without a slot is calculated at 2.81 GHz, which exactly matches the frequency obtained from simulations. In the next step (i.e. *Step-3*), a CSRR slot of length "$0.44\lambda_g$" (where λ_g is the guiding wavelength at 2.81 GHz) is etched on the top surface of each cavity. After introducing the CSRR slot, the resonant frequency shifts slightly around 2.7 GHz. This happens due to the increase in the path length for the surface current. Without a slot, there is a straight path from the feed to the radiating edges. However, after introducing a slot, the current must travel a longer path to complete a cycle. For maximum perturbation of the field, the CSRR slot (i.e., the center of the slot) is positioned at a distance of $0.5\lambda_g$ away from the point *O*. Later, it is observed by rotating the CSRR at various angles (0°–180°), the operating frequency can be continuously tuned towards the lower frequency [24]. When the split section of CSRR is facing point *O* (i.e., at 180°) the maximum miniaturization is achieved. The same has been demonstrated in Fig. 2. When the CSRR is placed at an angle of 0°, the electrical path length is the smallest while at angle $\theta = 180°$, the strong coupling takes place between the open edge current and CSRR slot that is responsible for increasing the electrical path, leading to lower operating frequency. The importance of the slot is to maintain the same isolation level by lowering the operating frequency [22]. The scalar electric field distribution has been shown in Fig. 2(a) and (b), when the corresponding port is excited while Fig. 2(c), represents S-parameters vs frequency plots with and without slots. The variation in the coupling of a field with the rotation of the slot can be better observed by the surface current in Fig. 3 (a), (b), (c). The

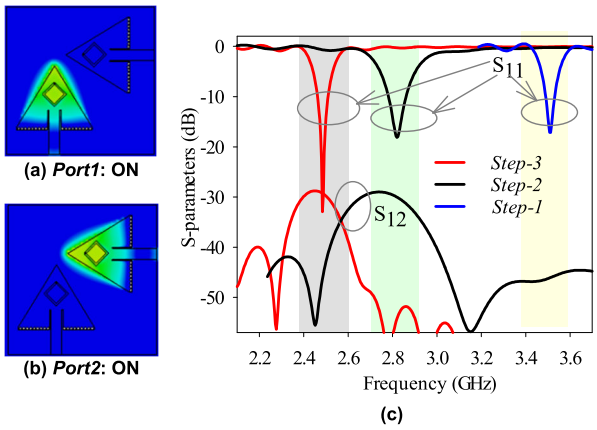

FIGURE 2. Absolute E- field at top metallic plane: Quarter-TE_{110} mode at 2.45 GHz (a) (*Port*1: ON), (b) (*Port*2: ON), (c) |S|-parameters for proposed MIMO-antenna without slot and with inclusion of CSRR at $\theta = 180°$.

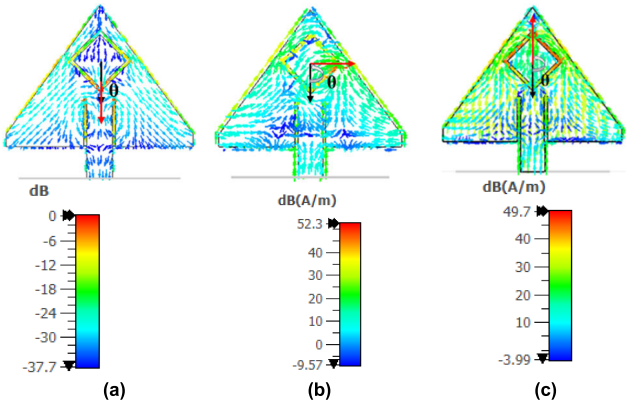

FIGURE 3. Vector surface current distribution at 2.45 GHz (a) $\theta = 0°$, (b) $\theta = 90°$, (c) $\theta = 180^0$.

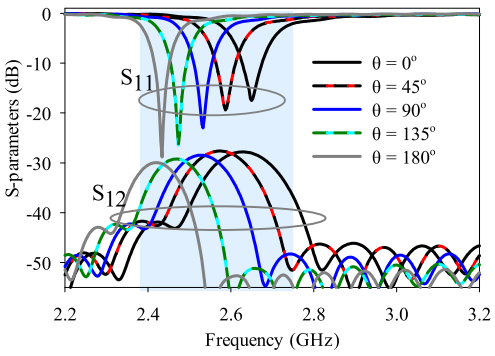

FIGURE 4. Variation of S-parameters with different rotation angle θ.

coupling of the field is maximum at $\theta = 180°$, and the current covers the largest path to achieve the maximum frequency shift. To achieve better decoupling, both antenna elements are placed in an orthogonal fashion that offers mutual coupling between ports more than 28 dB [22].

III. PARAMETRIC ANALYSIS

A CST 2022 simulation investigates how various parameters affect the frequency response. The variations of resonant

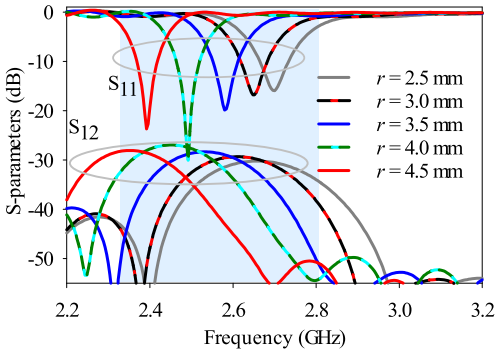

FIGURE 5. Variation of S-parameters with radius of the CSRR (r).

frequency with the rotation angle (θ), and radius (r) of the CSRR slot are discussed in this section. It can be observed from Fig. 4 that the resonant frequency decreases from 2.7-2.45 GHz if θ is varies in the range of 0°-180° [27]. Similarly, by varying the radius of CSRR in the range of 2.5-4.5 mm, the resonant frequency is shifted downward 2.75-2.4 GHz, as depicted in Fig. 5. Thus, either by rotating the slot with a fixed value of r or by increasing the value of r with fixed θ, the operating frequency can be tuned in a desired frequency range without altering the dimensions of the cavity. By increasing r, f_r decreases due to an increase in the reactive loading effect of the slot. Rotating the slot from 0° to 180° enhances isolation by about 2 dB due to increased field coupling through the slots.

A. EQUIVALENT CIRCUIT DIAGRAM

The equivalent circuit of the proposed antenna and its values of circuit elements (i.e., R, L, C) are extracted from the spice model of the CST solver, as illustrated in Fig. 6. The QMSIW behaves as a tank circuit at the resonant frequency, which is a parallel combination of resistance, capacitance, and inductance [7], [14]. With the addition of the CSRR slot, a capacitance C_m is added in the shunt, while the additional inductance L_s is incorporated due to the open edge aperture. The resistance R constitutes both input resistance and radiation resistance, those depend on the input impedance of the antenna as well as the characteristic impedance of the feedline. The impedance matching is governed by the inductance ratio of the impedance transformer. When Port1 is fed and Port2 is matched terminated or vice versa, the antenna resonates at 2.45 GHz. The total equivalent resistance (R_1), capacitance (C_{m1}), and inductance (L_{s1}) with Port1 excitation or (R_2, C_{m2}, L_{S2}) with Port2 excitation are shown in Fig. 6 (b). The circuit parameter values are extracted and mentioned in the table of Fig. 6. The equivalent circuit elements are consistent when one port is excited, and the other port is terminated with a matched load.

B. ON-BODY PERFORMANCE

The proposed antenna can be suitably used for WBAN scenarios, where wireless signals often encounter obstacles,

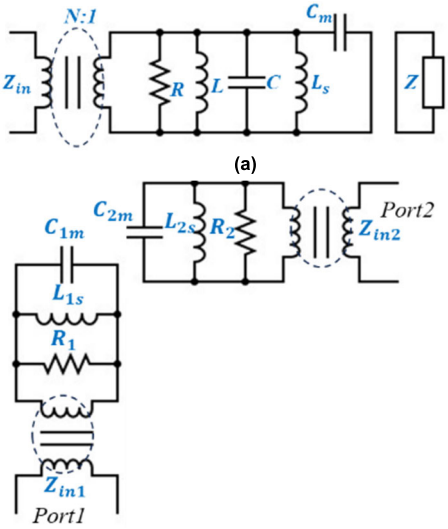

(b)

2.45 GHz	
$R_1 = R_2$ (Ω)	49.8
$L_{1s} = L_{2s}$ (nH)	0.15
$C_{1m} = C_{2m}$ (pF)	28.4
$C_{1m} = C_1 \| C_m$, $C_{2m} = C_2 \| C_m$, $L_{1s} = L_1 \| L_s$, $L_{2s} = L_2 \| L_s$, m represents mutual coupling, s represents shunt	

FIGURE 6. (a) Equivalent circuit model of single cavity antenna when any one port is excited, (b) Equivalent circuit model of proposed 2-element antenna, when both ports are excited.

interference, and body shadowing. The MIMO antennas can enhance the robustness of the communication link and minimize the effects of signal degradation [14]. In WBANs, where multiple devices may coexist in proximity, MIMO antennas can help reduce interference and improve the quality of communication links [18]. The safe exposure of radiation in WBAN environments is crucial.

The SAR value is verified on Hugo voxel body model in CST Microwave studio at the respective resonant frequency, if one port is excited and another port is matched terminated and vice versa. To decrease the simulation time, only a limited part of the Hugo voxel model has been taken into consideration [19], [20], as displayed in Fig. 7. Thus, the specific absorption rate (SAR) is calculated on all three body parts. As per the FCC guidelines for the safe exposure of radiation i.e., SAR $<$ 1.6 W/kg per 1 gm mass of the tissues. The maximum SAR values on arm, head and chest are obtained of 0.049 W/Kg, 0.108 W/Kg, 0.0524 W/kg, respectively for the fixed input power applied to the antenna 250mW. Hence, the suggested antenna sustains a low SAR value even under sufficient applied power, a result attributed to the utilization of QMSIW technology. Fig. 7(a) and (b) represent the SAR values on the arm, Fig. 7 (c) and (d) represent the SAR values on the head, and Fig. 7(e) and (f) signify the SAR values on the chest. The frequency response has been characterized in terms of S-parameters on the different parts of the human body such as arms, head, and chest in Fig. 8. It can be

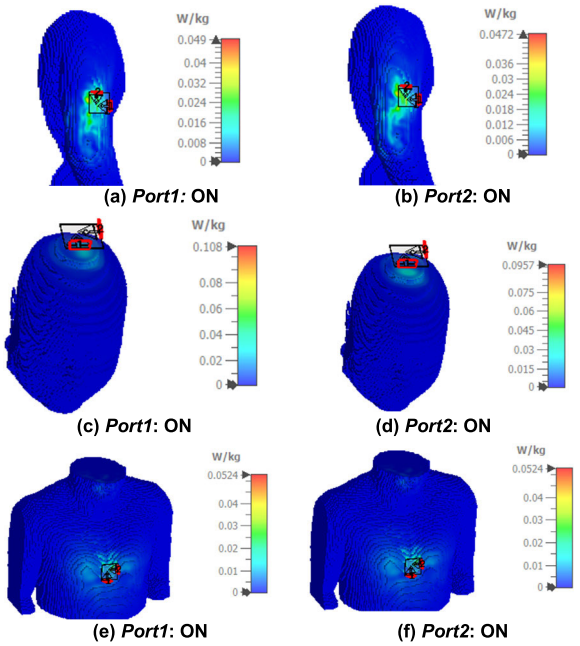

FIGURE 7. SAR vs frequency for different parts of the voxel body model, when one port is excited at a time (a) and (b) on the arm, (c) and (d) on the head, (e) and (f) on the chest.

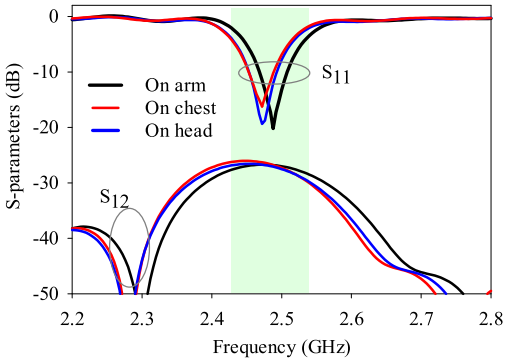

FIGURE 8. Proposed antenna on various parts of Hugo voxel model (a) on arms, head, chest.

observed that there is a minor variation observed in the S_{11} parameter with frequency for different body parts, while S_{21} remains below −28 dB.

C. DIVERSITY CHARACTERISTICS OF THE PROPOSED ANTENNA

The proposed 2-element MIMO antenna system supports spatial multiplexing and spatial diversity. Spatial diversity enhances reliability by transmitting data redundantly from multiple antennas. The performance metrics are evaluated in terms of envelope correlation coefficient (ECC), diversity gain (DG), mean effective gain (MEG), and channel capacity loss (CCL). The ECC assesses the correlation in radiation patterns between two distinct antennas. Ideally, it should be 0 [30], however, for most practical applications its value is typically < 0.5. The ECC can be calculated by using S-parameters as well as far-filed parameters. The ECC can be evaluated from S-parameters by using the equation (3) [14]

$$ECC = \frac{|S_{11*}S_{21} + S_{22} * S_{12}|^2}{\left(1 - \left(|S_{11}|^2 + |S_{21}|^2\right)\right)\left(1 - \left(|S_{22}|^2 + |S_{12}|^2\right)\right)} \tag{3}$$

In this case, with microstrip feedlines at *Port1* and *Port2*, ECC reaches a peak value of 0.025 from S-parameters. The ECC can also be determined by using far-field radiating field by using equation (4)

$$ECC = \frac{\left|\iint_0^{4\pi} \{\overline{E_1}(\theta,\phi) \cdot \overline{E_2}(\theta,\phi)\} d\Omega\right|^2}{\iint_0^{4\pi} \left|\overline{E_1}(\theta,\phi)\right|^2 d\Omega \iint_0^{4\pi} \left|\overline{E_1}(\theta,\phi)\right|^2 d\Omega} \tag{4}$$

where $\overline{E_1}(\theta,\phi) \cdot \overline{E_2}(\theta,\phi) = E_{\theta 1}(\theta,\phi)\, E^*_{\theta 2}(\theta,\phi) + E_{\phi 1}(\theta,\phi)\, E^*_{\phi 2}(\theta,\phi)$

Where $\overline{E_1}(\theta, \phi)$ is the electric field in far-field region when *Port1* is excited while *Port2* is terminated with matched load, $\overline{E_2}(\theta, \phi)$ is the electric field in far-field region when *Port2* is excited while *Port1* is terminated with matched load. From far-field parameters, the ECC value is determined as 0.02 [28].

To ensure the reliability of communication channels, it is crucial to examine the diversity gain (DG), which quantifies the increase in antenna gain achieved by incorporating several antennas [14]. By integrating many antennas into the MIMO configuration, the DG value reaches 9.8 dB, as shown in Fig. 9, which is precise to the desired value of 10 dB, and it can be obtained by using (5) [30], [31] shown below:

$$DG = 10\sqrt{1 - |0.99\, Ecc|^2} \tag{5}$$

An additional crucial parameter for assessing antenna diversity performance is the mean effective gain (MEG), representing the ratio of mean received power to mean transmitted power. The proposed antenna achieves an MEG of approximately −3.07 dB, closely approaching the acceptable standard MEG result should fall within the range of –3 dB to –12 dB [31]. The calculations for MEG can be performed using specific equations outlined in [14].

Another crucial parameter to define MIMO diversity performance is Channel Capacity Loss (CCL). It refers to the reduction in the maximum achievable data rate or throughput of the MIMO system compared to the ideal case without channel impairments. For the proposed 2-port MIMO antenna, channel capacity losses (i.e. CCL) can be calculated by using equation (6)

$$\mathrm{CCL_{loss}} = -\log_2 \det(\psi^R) \tag{6}$$

where ψ^R is the correlation matrix of the receiving antenna and for 2-ports, it can be expressed as

$$\psi^R = \begin{pmatrix} \psi_{11} & \psi_{12} \\ \psi_{21} & \psi_{22} \end{pmatrix}$$

$$\psi_{ii} = 1 - \left(|S_{11}|^2 + |S_{12}|^2\right)$$

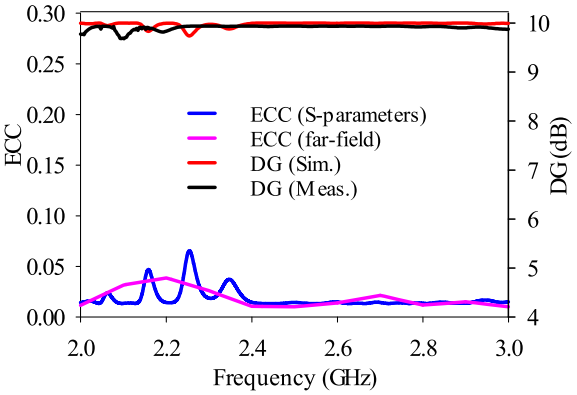

FIGURE 9. ECC and DG against frequency plots.

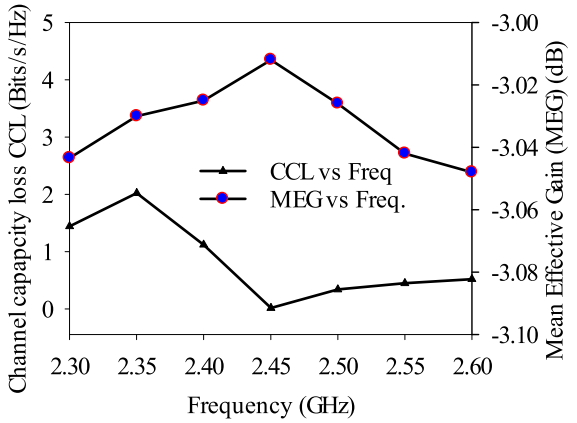

FIGURE 10. CCL and MEG against frequency plots.

$$\psi_{ij} = -(S_{11} * S_{12} + S_{21} * S_{22})$$
$$\psi_{ji} = -(S_{21} * S_{22} + S_{11} * S_{12})$$
$$\psi_{jj} = 1 - \left(|S_{22}|^2 + |S_{21}|^2\right)$$

The CCL and MEG vs frequency plots are depicted in Fig. 10. The Channel capacity loss is calculated as 0.02 bits/s/Hz at the resonant frequency that is less than the typical expected value < 0.4 bits/s/Hz.

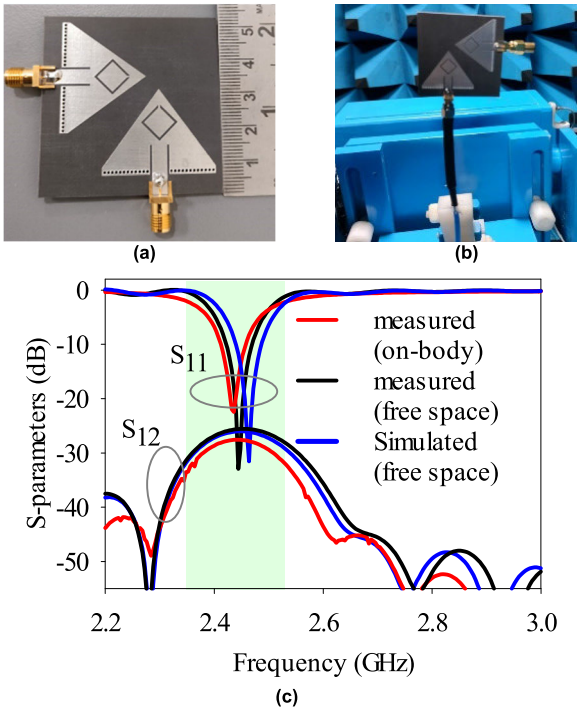

FIGURE 11. Fabricated prototype of the proposed MIMO antenna (a) top view, (b) antenna under test, (c) simulated and measured S-parameters plots vs frequency in free space conditions and on-body scenario.

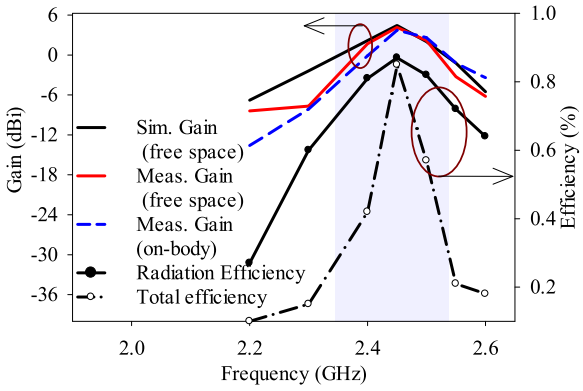

FIGURE 12. Simulated and measured gain and efficiency plots in free space/on-body.

IV. MEASUREMENT RESULTS

The envisioned antenna is fabricated on RT Duroid 5880 laminate of dielectric constant ($\varepsilon_r = 2.2$) and loss tangent ($\tan\delta = 0.009$) with a thickness of 1.574 mm. Utilizing the conventional printed circuit board (PCB) methodology, the antenna undergoes prototyping. A series of via holes, each with a diameter of 0.8 mm, is incorporated using the plated-through technique (PTH) [14]. The photograph of the fabricated prototype is shown in Fig. 11(a). To validate the effectiveness of the proposed design, the antenna prototype undergoes experimental testing with the help of Vector Network Analyzer model MS-46122B inside the anechoic chamber, illustrated in Fig. 11(b). To measure on-body parameters, pork muscle tissues that emulate properties of human muscle body tissues as dielectric constant (ε_r) = 35.8 and conductivity (σ) = 1.2 S/m at 2.45 GHz [23] have been considered to carry out on-body measurements. Pork tissues are often used in scientific experiments as they have a composition and structure that is relatively like human muscle tissues. A similarity between the measured and simulated S-parameters is illustrated in Fig. 11(c), demonstrating a good agreement among the responses.

The S-parameter responses are obtained by feeding one port while loading another port with a matched load. The simulated (measured) minimum isolation levels at the resonant frequencies, 2.45 GHz (2.44 GHz), are found to be better than 28 dB (28.5 dB), respectively. The simulated and measured

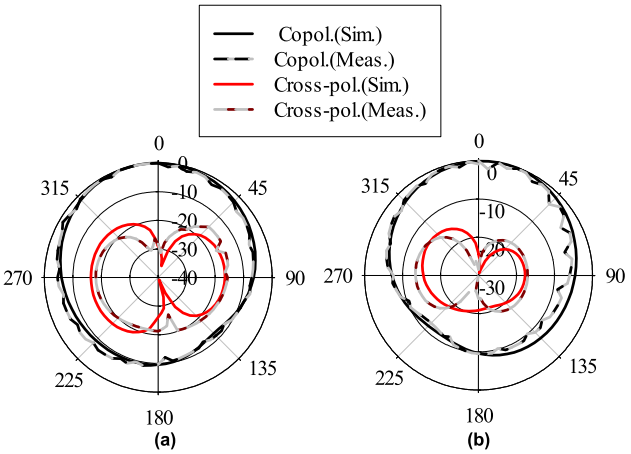

FIGURE 13. Simulated and measured radiation patterns at 2.45 GHz (a) H-plane ($\phi = 90°$), and (b) E-plane ($\phi = 0°$).

plots for gain and efficiency have been plotted in Fig. 12. The simulated value of gain is achieved of 4.35 dBi while the measured value of gain is 4.2 dBi, including all losses, (i.e. substrate, connectors, and feeding losses) respectively. Without incorporating losses, the peak value of gain is achieved of 5.0 dBi. The 0.8 dB losses are contributing predominantly due to a drop in total efficiency by around 15%, than the ideal expected value of 100%. The simulated gain on the voxel body model is achieved of 4.4 dBi while on-pork tissues it is obtained of 4.25 dBi, which is close to the free space condition. confirming the stable radiating characteristics in the proximity of the body scenario. The radiation efficiency of the proposed antenna at the operating frequency is achieved of 87.5 %, while the total efficiency is obtained of 85.6 %. The normalized radiation patterns at the cut planes $\phi = 0°$ and $\phi = 90°$ are depicted at 2.45 GHz in Fig. 13. Both simulations and experiments show unidirectional radiation patterns due to the cavity-backing structure, mostly directed broadside. The cross-polar levels in the broadside direction are observed to be below -20 dB, and the FTBR exceeds 10 dB at 2.45 GHz.

To emphasize the importance of the proposed design, a comparison of different parameters of the MIMO antenna with other reported works [11], [12], [13], [14], [15], [16], [17], [18], [19], [20], [21], [22], [23], [24], [25], [26], [27], [28], [29] is presented in Table 1. The proposed design exhibits a more compact size (defined in terms of guided wavelength at dominate mode), planar configuration, better isolation, and a comparable value of directive gain within the operating frequency band. Additionally, the proposed MIMO antenna offers scalability to different frequency bands by adjusting the radius and angle of the CSRR-slot by keeping the dimensions of the cavity fixed. The proposed design shows slightly lower value of isolation as compared to the work presented in [13], [15], [16], and [20], however the size of the proposed antenna is substantially compact. Moreover, the uniqueness of the proposed antenna stems from its simple and straightforward design, which yield substantial inherent isolation without necessitating the application of specialized decoupling techniques.

TABLE 1. Comparison of 4-port MIMO antenna with other existing works.

Para.	f_r (GHz)	Directi. Gain (dBi)	Feeding method/ Spacing between elements (mm)	Isolation (dB)	Total Size in (Electrical length)	No. of ele.
[11]	2.1	4.3	Microstrip / 50	25	1.43 λ_g ×0.9 λ_g	2×2
[12]	3.51	4.9	Coaxial / 2	19.5	0.9 λ_g × .9λ_g	1×1
[13]	3.5	4.1	Coaxial / ≈ 18	30	0.7 λ_g × 0.7 λ_g	1×1
[15]	5.8	3.5	Microstrip / 1	25	1.25 λ_g ×1.2λ_g	1×1
[16]	5.9	5.5	Microstrip / 10.4	31	1.2 λ_g×1.2 λ_g	1×1
[17]	2.63	5.5	Coaxial / 22	17	1.5 λ_g ×1.5 λ_g	2×2
[18]	5.8	6	Microstrip / 14.4	17	2.6 λ_g ×1.7 λ_g	1×1
[19]	5.8	3.2	Microstrip / 7	24.5	1.5 λ_l×1.7λ_l	1×1
[20]	5.9	6.2	Microstrip / 30	40	2.6 λ_g ×2.6 λ_g	2×2
[22]	3.5	4.6	Coaxial / 1.3	18	0.8 λ_l×0.68 λ_l	1×1
[25]	2.45 / 3.5	2.4 / 3.4	Coaxial / N.A.	19.2	0.7 λ_g×1.7 λ_g	1×1
[26]	3.5	N.A.	Coaxial / 25	30	≈2.3 λ_g×2.3 λ_g	1×1
[29]	6	4.72	Coaxial / 7	21	7.4 λ_g^2	8
This work	2.45	5.0	Microstrip / 5	28.5	0.6 λ_g × 0.6 λ_g	1×1

* $\lambda_{g\,is}$ the guide wavelength at the dominant mode operating frequency.

V. CONCLUSION

This article presents a compact 2-ports MIMO antenna operating at 2.45 GHz, within the ISM frequency band. By capitalizing on the symmetrical nature of the dominant mode (TE_{110}), miniaturization is achieved in the QMSIW cavity, resulting in a 75% reduction compared to the FMSIW cavity. To further enhance compactness, a diamond shaped CSRR slot is introduced on the top of each cavity, reducing the size by approximately 13%. Moreover, the slot allows continuous frequency variation by rotating it at different angles. The orthogonal placement of cavities offers superior isolation (>28 dB) in both ports. The antenna boasts a highly compact and low-profile design, enabling easy integration with planar circuits integrated with microstrip feedlines. MIMO properties, such as ECC and DG, MEG, CCL are calculated and found to be at satisfactory levels. The

proposed antenna configuration offers reliable communication in a complex WBAN environment, thanks to its MIMO capabilities. Moreover, the compactness, reliable communication, and simple and low-profile structure make it the optimal choice in WBAN application.

REFERENCES

[1] M. A. Jensen and J. W. Wallace, "A review of antennas and propagation for MIMO wireless communications," *IEEE Trans. Antennas Propag.*, vol. 52, no. 11, pp. 2810–2824, Nov. 2004.

[2] D. Gesbert, M. Kountouris, R. W. Heath Jr., C.-B. Chae, and T. Salzer, "Shifting the MIMO paradigm: From single user to multiuser communications," *IEEE Signal Process. Mag.*, vol. 24, no. 5, pp. 36–46, Oct. 2007.

[3] X. Q. Lin, H. Li, S. He, and Y. Fan, "A decoupling technique for increasing the port isolation between two closely packed antennas," in *Proc. IEEE Int. Symp. Antennas Propag.*, Jul. 2012, pp. 1–2.

[4] Y. Hao and C. G. Paini, "Isolation enhancement of anisotropic UC-PBG microstrip diplexer patch antenna," *IEEE Antennas Wireless Propag. Lett.*, vol. 1, pp. 135–137, 2002.

[5] M. S. Sharawi, "Printed multi-band MIMO antenna systems and their performance metrics [wireless corner]," *IEEE Antennas Propag. Mag.*, vol. 55, no. 5, pp. 218–232, Oct. 2013.

[6] A. Kumar and A. A. Althuwayb, "SIW resonator-based duplex filtenna," *IEEE Antennas Wireless Propag. Lett.*, vol. 20, pp. 2544–2548, 2021.

[7] A. Iqbal, J. J. Tiang, C. K. Lee, and N. K. Mallat, "SIW cavity backed self-diplexing tunable antenna," *IEEE Trans. Antennas Propag.*, vol. 69, no. 8, pp. 5021–5025, Aug. 2021.

[8] I. Rosaline, A. Kumar, P. Upadhyay, and A. H. Murshed, "Four element MIMO antenna systems with decoupling lines for high-speed 5G wireless data communication," *Int. J. Antennas Propag.*, vol. 2022, Jun. 2022.

[9] W. A. Ali, A. A. Ibrahim, and A. E. Ahmed, "Dual-band millimeter wave 2×2 MIMO slot antenna with low mutual coupling for 5G networks," *Wireless Pers. Commun.*, vol. 129, pp. 2959–2976, Mar. 2023.

[10] S. Yan, P. J. Soh, and G. A. E. Vandenbosch, "Dual-band textile MIMO antenna based on substrate-integrated waveguide (SIW) technology," *IEEE Trans. Antennas Propag.*, vol. 63, no. 11, pp. 4640–4647, Nov. 2015.

[11] M. Ikram, R. Hussain, A. Ghalib, and M. S. Sharawi, "Compact 4-element MIMO antenna with isolation enhancement for 4G LTE terminals," in *Proc. IEEE Int. Symp. Antennas Propag. (APSURSI)*, Jun. 2016, pp. 535–536.

[12] B. Niu and J. Tan, "Compact SIW cavity MIMO antenna with enhanced bandwidth and high isolation," *Electron. Lett.*, vol. 55, no. 11, pp. 631–632, May 2019.

[13] S. Nandi and A. Mohan, "A compact eighth-mode circular SIW cavity-based MIMO antenna," *IEEE Antennas Wireless Propag. Lett.*, vol. 20, pp. 1834–1838, 2021.

[14] B. Pramodini, D. Chaturvedi, and G. Rana, "Design and investigation of dual-band 2×2 elements MIMO antenna-diplexer based on half-mode SIW," *IEEE Access*, vol. 10, pp. 79272–79280, 2022.

[15] M. N. Abbasi, A. Aziz, K. Aljaloud, A. R. Chishti, Y. T. Aladadi, and R. Hussain, "A proximity 2-element MIMO antenna using optically transparent wired-metal mesh and polyethylene terephthalate material," *IEEE Access*, vol. 11, pp. 78811–78819, 2023.

[16] P. Kumari and S. Das, "A MIMO antenna system using self-decoupled EMSIW dual-beam antenna elements," *IEEE Access*, vol. 10, pp. 1339–1345, 2022.

[17] K. Ding, C. Gao, D. Qu, and Q. Yin, "Compact broadband MIMO antenna with parasitic strip," *IEEE Antennas Wireless Propag. Lett.*, vol. 16, pp. 2349–2353, 2017.

[18] S. S. Jehangir and M. S. Sharawi, "A miniaturized UWB biplanar yagi-like MIMO antenna system," *IEEE Antennas Wireless Propag. Lett.*, vol. 16, pp. 2320–2323, 2017.

[19] A. Iqbal, O. A. Saraereh, A. Bouazizi, and A. Basir, "Metamaterial-based highly isolated MIMO antenna for portable wireless applications," *Electronics*, vol. 7, no. 10, p. 267, Oct. 2018.

[20] D. Gangwar, J. Malik, and A. Patnaik, "Enhanced isolation 4×4 MIMO antennas on cross-substrate for vehicular communications," *IEEE Antennas Wireless Propag. Lett.*, vol. 22, pp. 2715–2719, 2023, doi: 10.1109/LAWP.2023.3314212.

[21] N. C. Pradhan, K. S. Subramanian, R. K. Barik, and Q. S. Cheng, "A shielded-QMSIW-based self-diplexing antenna for closely spaced bands and high isolation," *IEEE Antennas Wireless Propag. Lett.*, vol. 20, pp. 2382–2386, 2021.

[22] B. Niu and J. Tan, "Compact self-isolated MIMO antenna system based on quarter-mode SIW cavity," *Electron. Lett.*, vol. 55, no. 10, pp. 574–576, May 2019.

[23] D. Chaturvedi and S. Raghavan, "Circular quarter-mode SIW antenna for WBAN application," *IETE J. Res.*, vol. 64, no. 4, pp. 482–488, Jul. 2018.

[24] D. Chaturvedi and A. Kumar, "A QMSIW cavity-backed self-diplexing antenna with tunable resonant frequency using CSRR slot," *IEEE Antennas Wireless Propag. Lett.*, vol. 23, pp. 259–263, 2024.

[25] S. Zhang, B. K. Lau, Y. Tan, Z. Ying, and S. He, "Mutual coupling reduction of two PIFAs with a T-shape slot impedance transformer for MIMO mobile terminals," *IEEE Trans. Antennas Propag.*, vol. 60, no. 3, pp. 1521–1531, Mar. 2012.

[26] F. Liu, J. Guo, L. Zhao, G.-L. Huang, Y. Li, and Y. Yin, "Ceramic superstrate-based decoupling method for two closely packed antennas with cross-polarization suppression," *IEEE Trans. Antennas Propag.*, vol. 69, no. 3, pp. 1751–1756, Mar. 2021.

[27] S. Sam and S. Lim, "Electrically small eighth-mode substrate-integrated waveguide (EMSIW) antenna with different resonant frequencies depending on rotation of complementary split ring resonator," *IEEE Trans. Antennas Propag.*, vol. 61, no. 10, pp. 4933–4939, Oct. 2013.

[28] S. A. Ali, M. Wajid, A. Kumar, and M. S. Alam, "Design challenges and possible solutions for 5G SIW MIMO and phased array antennas: A review," *IEEE Access*, vol. 10, pp. 88567–88594, 2022.

[29] M. Mishra, S. Chaudhuri, R. S. Kshetrimayum, M. S. Sharawi, and A. A. Kishk, "A highly efficient & low-mutual coupling partial $\pi/8$ SIW cavity based 8-port MIMO antenna," *IEEE Antennas Wireless Propag. Lett.*, vol. 22, no. 7, pp. 1721–1725, Mar. 2023.

[30] H. H. Gerami, R. Kazemi, and A. E. Fathy, "Development of a metasurface-based slot antenna for 5G MIMO applications with minimized cross-polarization and stable radiation patterns through mode manipulation," *Sci. Rep.*, vol. 14, no. 1, p. 8016, Apr. 2024.

[31] M. A. Sufian, N. Hussain, and N. Kim, "Quasi-binomial series-fed array for performance improvement of millimeter-wave antenna for 5G MIMO applications," *Eng. Sci. Technol., Int. J.*, vol. 47, Nov. 2023, Art. no. 101548.

DIVYA CHATURVEDI (Senior Member, IEEE) was born in Kanpur, India. She received the B.Tech. degree in electronics and communication engineering from Uttar Pradesh Technical University, India, in 2011, the M.Tech. degree in electronics engineering from Pondicherry Central University, India, in 2015, and the Ph.D. degree in substrate-integrated waveguide-based cavity-backed antenna from the National Institute of Technology, Tiruchirappalli, in 2019. Currently, she is an Assistant Professor with SRM University-AP, Amaravati. She is also an active Researcher in substrate-integrated waveguide antennas, filters, beam forming antennas, wearable antennas, and biological effects of radiation on human body. She has published several articles on SIW self-multiplexing antennas of IEEE TRANSACTIONS ON ANTENNAS AND PROPAGATION (IEEE TAP), IEEE ANTENNAS AND WIRELESS PROPAGATION LETTERS (IEEE AWPL), RFCAD, and *IET MAP* journals.

PRAKASH JADHAV is currently pursuing the Ph.D. degree in mechanical engineering with the University of Mississippi, USA. He is also a Professor in mechanical engineering with SRM University-AP, Andhra Pradesh. He has over 25 years of versatile experience in academics, research, and industry. His core research interests include design, computational mechanics and experimental mechanics applied to automotive, and aerospace and other applications. He has published over 40 articles in international journals and conferences.

AYMAN A. ALTHUWAYB (Member, IEEE) received the B.Sc. degree (Hons.) in electrical engineering (electronics and communications) from Jouf University, Saudi Arabia, in 2011, the M.Sc. degree in electrical engineering from California State University, Fullerton, CA, USA, in 2015, and the Ph.D. degree in electrical engineering from Southern Methodist University, Dallas, TX, USA, in 2018. He is currently an Assistant Professor with the Department of Electrical Engineering, Jouf University, Saudi Arabia. His current research interests include antenna, design and propagation, microwaves and millimeter waves, wireless power transfer, ultrawideband and multiband antennas, and filters.

KHALED ALIQAB (Member, IEEE) was born in Sakaka, Saudi Arabia, in 1990. He received the B.Eng. degree (Hons.) in electrical and electronic engineering, the M.Sc. degree (Hons.) in mobile communications, and the Ph.D. degree in electrical engineering from Heriot-Watt University, Edinburgh, U.K., in 2015 and 2021, respectively. He is currently an Assistant Professor with the Department of Electrical Engineering, Jouf University, Sakaka, Saudi Arabia. His current research interests include advanced miniature multilayer self-packaged components, balanced differential circuit design, advanced radio frequency (RF)/microwave device technologies, liquid-crystal polymer (LCP) material, metamaterials, 3-D printing, wireless communication radar and satellite applications, low power, low-cost wireless sensor networks, and energy harvesting, and biomedical sensors and applications.